Geomechanics and Engineering, *Vol. 37, No. 4 (2024) 341-358*
https://doi.org/10.12989/gae.2024.37.4.341

Effects of reinforcement on two-dimensional soil arching development under localized surface loading

Geye Li[1a], Chao Xu[2], Panpan Shen*[3], Jie Han[4] and Xingya Zhang[5]

[1]*Department of Civil Engineering, School of Environment and Safety Engineering, North University of China, Taiyuan, Shanxi Province, China*
[2]*Key Laboratory of Geotechnical and Underground Engineering of Ministry of Education, Department of Geotechnical Engineering, College of Civil Engineering, Tongji University, Shanghai, China*
[3]*Shanghai Investigation, Design & Research Institute Co., Ltd., Shanghai, China*
[4]*Department of Civil, Environmental, and Architectural Engineering, the University of Kansas, Lawrence, KS, USA*
[5]*Seazen Holdings Co., Ltd., Shanghai, China*

(*Received June 24, 2022, Revised April 20, 2024, Accepted April 25, 2024*)

Abstract. This paper reports several plane-strain trapdoor tests conducted to investigate the effects of reinforcement on soil arching development under localized surface loading with a loading plate width three times the trapdoor width. An analogical soil composed of aluminum rods with three different diameters was used as the backfill and Kraft paper with two different stiffness values was used as the reinforcement material. Four reinforcement arrangements were investigated: (1) no reinforcement, (2) one low stiffness reinforcement R1, (3) one high stiffness reinforcement R2, and (4) two low stiffness reinforcements R1 with a backfill layer in between. The stiffness of R2 was approximately twice that of R1; therefore, two R1 had approximately the same total stiffness as one R2. Test results indicate that the use of reinforcement minimized soil arching degradation under localized surface loading. Soil arching with reinforcement degraded more at unloading stages as compared to that at loading stages. The use of stiffer reinforcement had the advantages of more effectively minimizing soil arching degradation. As compared to one high stiffness reinforcement layer, two low stiffness reinforcement layers with a backfill layer of certain thickness in between promoted soil arching under localized surface loading. Due to different states of soil arching development with and without reinforcement, an analytical multi-stage soil arching model available in the literature was selected in this study to calculate the average vertical pressures acting on the trapdoor or on the deflected reinforcement section under both the backfill self-weight and localized surface loading.

Keywords: arching effect; cyclic loading; reinforcement; static repetitive loading; trapdoor

1. Introduction

Terzaghi (1943) described soil arching effect as "one of the most universal phenomena encountered in soils both in the field and in the laboratory". Soil arching commonly exists when soil interacts with structural elements, for example, tunnels, retaining walls, pipelines, and piles. It is defined as transfer of a load from the yielding soil mass portion onto the adjoining stationary portions (also called supports) in response to a relative displacement between these two portions. Soil arching effect can be classified into two categories according to the direction of shear stresses generated in soil: (1) "positive soil arching" when the yielding mass moves downward relative to the stationary portions and upward shear stresses are generated in the soil and (2) "negative soil arching" when the soil movement and the generated shear stresses are on the opposite directions to those for "positive soil arching". This study focused on the positive soil arching induced by movement of a single rigid trapdoor, which results in a decrease of vertical stresses on the yielding portion and an increase of vertical stresses on the stationary portion. In transportation engineering applications, positive soil arching may result from: (1) underground cavities resulting from engineering excavation (e.g., tunnels, pipelines, mines), (2) localized or differential settlement encountered in piled embankments, and (3) underground sinkholes induced by karstic erosion.

Numerous studies have been conducted to investigate soil arching effect without geosynthetic reinforcement under backfill self-weight (Terzaghi 1936, McNulty 1965, Ladanyi and Hoyaux 1969, Iglesia 1991, Jenck *et al.* 2005, 2007, Chevalier and Otani 2011, Chevalier *et al.* 2012, Moradi and Abbasnejad 2015, Rui *et al.*2016a, b, Han *et al.* 2017, Bhandari and Han 2018, Lai *et al*. 2020, Nguyen and Tran 2021) and under uniform surcharge (Lai *et al.* 2014, Rui *et al*. 2020, Liang *et al*. 2020). However, soil arching may degrade and even collapse under localized surface loading, e.g., static loading caused by structure dead loads or dynamic loads (e.g., traffic live loads). So far a few studies have been carried out to investigate soil arching under localized surface loading without geosynthetic reinforcement (Heitz *et al.* 2008, Han *et al*. 2015, Al-Naddaf *et al*. 2017, 2019b, Xu *et al*. 2019, Zhang *et al.*

*Corresponding author, Senior Engineer
E-mail: hermit_shpp@hotmail.com
[a]Lecturer
E-mail: 20230210@nuc.edu.cn

ISSN: 2005-307X (Print), 2092-6219 (Online)

2021a, b). For example, Han *et al.* (2015) carried out cylinder trapdoor model tests to investigate soil arching under localized dynamic loading. Collapse of soil arching occurred when the ratio of the embankment height to the hole diameter (i.e., trapdoor width) was less than three. Al-Naddaf *et al.* (2017, 2019b) investigated soil arching degradation subjected to localized surface loading under a plane-strain condition using trapdoor tests and found that the localized surface load reduced the degree of soil arching when the trapdoor normalized displacement was1.5%. Xu *et al.* (2019) conducted a series of trapdoor tests to investigate soil arching subject to static and cyclic loading. Their results indicated that the degradation of soil arching induced by surface loading became more significant with the increase of the applied pressures and the frequency of cyclic loading. Zhang *et al*. (2021a, b) investigated soil arching above multiple buried flexible structures subjected to cyclic loading using plane-strain trapdoor tests with transparent sand. Their study clearly showed that localized cyclic loading accelerated the degradation or collapse of soil arching. Therefore, more attention should be paid to the development or degradation of soil arching under localized surface loading.

In the past few decades, geosynthetic has been widely used as soil reinforcement layers in engineering practices (Mittal and Meyase 2012, Jesmani *et al*. 2016, Won *et al.* 2016, Liu *et al.* 2017, Rebello *et al*. 2018, Biradar *et al.* 2019, Xu *et al.* 2020, Kahyaoglu *et al*. 2021). Particularly, geosynthetic reinforcement has been employed to minimize degradation of soil arching under backfill self-weight and uniform surcharge (e.g., Giroud *et al.* 1990, Wang *et al.* 2009, Eskişar *et al.* 2012, Xu *et al*. 2016, Feng *et al.* 2017, Balaban and Onur 2018, Rui *et al.* 2019). More recently, geosynthetic reinforcement has been successfully utilized to minimize the degradation of soil arching under localized surface loading. Heitz *et al*. (2008) carried out model tests to investigate soil arching under different loading conditions. Their results indicated that cyclic loading caused more soil arching degradation than static loading and the use of a geogrid reduced the degradation of soil arching caused by both static and cyclic loads. Bhandari (2010) conducted numerical studies to investigate the effect of a localized cyclic load on soil arching using the discrete element method and found that cyclic loading minimized soil arching but geosynthetic reinforcement stabilized soil arching. Huckert *et al.* (2016) performed full-scale experiments to study soil arching during formation and under static and cyclic loading on embankments with different reinforcement conditions. Their results showed that the reinforcement reduced the settlement at the top of the embankment under cyclic loading. Al-Naddaf *et al*. (2019b) investigated soil arching with and without geosynthetic reinforcement subjected to localized surface static loads using trapdoor model tests and found that the reinforcement helped maintain soil arching under loading. Aqoub *et al.* (2020) conducted model tests to investigate the behavior of unreinforced and reinforced piled low embankments under cyclic loading. The benefit of the reinforcement was obvious on the load transfer mechanism and the surface settlement. However, limited studies have focused on the effects of reinforcement properties, such as tensile stiffness or strength, on the development of soil arching under localized surface loading. In addition, most studies on soil arching in geosynthetic-reinforced fill only employed a single reinforcement layer despite the fact that double or multiple reinforcement layers are commonly used in the field. Therefore, further studies are necessary to investigate the effects of reinforcement on the development of soil arching under localized surface loading, which is important for engineering practices.

In this study, a two-dimensional (2D) trapdoor apparatus developed by Xu *et al*. (2019) was used to investigate the effects of reinforcement on the development of soil arching under localized surface loading with a loading plate width three times the trapdoor width. Four different reinforcement arrangements were utilized in this study, which included different reinforcement stiffness and number of reinforcement layers. Trapdoor tests under backfill self-weight were first conducted so that baseline results could be obtained. Trapdoor tests under static repetitive and cyclic loading were then conducted to investigate the effects of localized surface loading on the development of soil arching with different reinforcement arrangements. Finally, the results of trapdoor tests under both backfill self-weight and under localized surface loading are compared to two analytical soil arching models for estimating additional average vertical pressures acting on the trapdoor or on the deflected reinforcement section induced by localized surface loading. The purpose of using two different analytical models was to consider the effects of reinforcement on the evolution of soil arching.

2. Experimental setup

2.1 Test apparatus

A 2D trapdoor apparatus developed by Xu *et al.* (2019), as shown in Fig. 1, was used in this study. The apparatus consists of a platform, a test box, a reaction frame, and a servo loading system. The inner width of the test box was 900 mm. Seven hardwood blocks (B1 to B7) with a width B of 128 mm and an out-of-plane thickness d of 50 mm were installed at the bottom of the box. There was a gap of 0.5 mm wide between adjacent blocks to avoid friction. Seven "S-shape" load cells with a resolution of 0.01 kg were mounted under these seven blocks to measure the force (F_t) applied onto each block. These seven blocks could be moved upwards and downwards independently by electric motors, which were connected to a control box. The control box could control and record the displacements of the blocks. The inner out-of-plane thickness of the test box was 51 mm, which was slightly larger than that of the blocks; therefore, the friction between the blocks and the front and back side walls of the box could be avoided. The front wall of the test box was made of a transparent Plexiglas panel, thus allowing direct visual observation of backfill deformations. A high-speed camera was placed in front of the test box to take photos of the front section during the tests. The digital photos were processed using the 2D

particle image velocimetry (PIV) technique (White *et al.* 2003) to acquire the displacement field of the backfill and the deformation of the reinforcement. To reduce possible friction effects, the left and right side walls of the test box were covered with Teflon membranes.

During the trapdoor tests under localized surface loading, an electric servo system with the highest frequency of 20 Hz and a force resolution of 1 N was used to apply surface static repetitive and cyclic loads through the loading plate with a width $L = 3B = 384$ mm (B is the trapdoor width) and an out-of-plane thickness d of 50 mm. The force applied on the loading plate was monitored during the tests to ensure the consistency between the input and output. In this study, static repetitive loading is referred to a loading process that a load is applied, maintained for a certain time, and then released (i.e., unloaded). This process is different from cyclic loading in which a load is applied and released at a certain frequency. Alternatively, static repetitive loading can be considered as cyclic loading at a frequency close to 0.

2.2 Test backfill

Analogical soils (e.g., aluminum or steel rods) have been increasingly used by researchers to create a plane-strain condition in model tests because it can eliminate the negative effects of side wall friction induced by the granular soil on test results while retaining most important characteristics of the granular soil and exhibiting simpler mechanical behavior (Ladanyi and Hoyaux 1969). Side wall friction in the test box interferes with the movement of the granular soil. As a result, the accuracy or reliability of some test results, such as the backfill displacement contour and the deformation of the reinforcement achieved by the PIV technique, are significantly impacted and additional efforts are needed to evaluate or eliminate these negative effects. In addition, using analogical soils has the advantages of easy construction and hence better repeatability. Therefore, an analogical soil composed of aluminum rods with different diameters was used as the backfill in this study to create a plane-strain condition. Many studies have been conducted in the past to evaluate soil arching by successfully using analogical soils to model the behavior of actual soils under both static and cyclic loading (Jenck *et al.* 2007, Bhandari 2010; Bhandari and Han 2018, Rui *et al*. 2019, 2020, Xu *et al.* 2019, Bao *et al*. 2021). No significant differences were observed in terms of their behavior using analogical soils and actual soils. For example, Rui *et al*. (2020) investigated the load transfer mechanism of granular cushions between column foundations and rigid rafts by using both sand and analogical soil. The comparison of their test results using these two materials demonstrated that the analogical soil reasonably simulated the behavior of the sand in terms of both deformations and stresses. Xu *et al*. (2019) showed that cyclic loading caused more degradation of soil arching than static loading by using the same analogical soil as used in this study. Same results were found by Zhang *et al.* (2021a) by using a transparent sand. Moreover, Xu *et al*. (2019) concluded that higher cyclic loading frequency caused more soil arching degradation, which was similar to

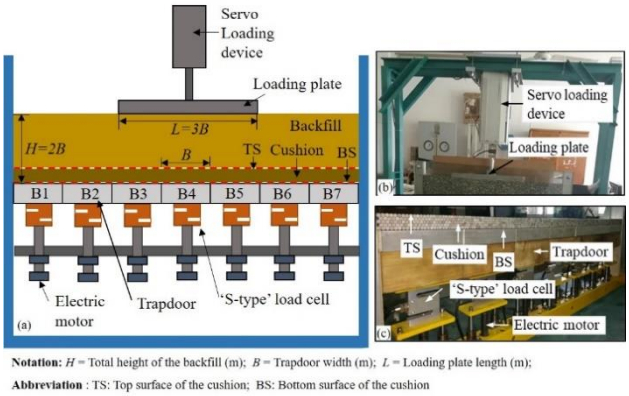

Fig. 1 Trapdoor apparatus used in this study from Xu *et al.* (2019): (a) schematic of the trapdoor setup, (b) photo of the loading device and (c) photo of the test box

those found by Zhang *et al*. (2021a) and Bi *et al.* (2020) by using actual sands. Therefore, it can be concluded that the analogical soil used by Xu *et al.* (2019) and this study could reasonably simulate the behavior of actual sand under cyclic loading in terms of soil arching developments.

The aluminum rods had three different diameters of 3, 4, and 5 mm and were mixed in a mass ratio of 1:1:1. The unit weight of the backfill γ was 22.4 kN/m^3. All the aluminum rods had a length of 50 mm, which is the same as the thickness of the hardwood blocks d. The friction angle ϕ of the backfill determined through biaxial compression tests (Xu *et al.* 2019) was 25°, which is lower than that of typical natural sand but is close to the friction angles of similar materials reported in other studies (Ladanyi and Hoyaux 1969, Han *et al*. 2012). Below the backfill, five layers of aluminum rods with a uniform diameter of 5 mm were laid on top of the blocks to create a load-transfer cushion, which ensured uniform force transfer from the aluminum rods to the load cells. The cushion thickness h was approximately 22.4 mm, as shown in Fig. 1. The ratio of the cushion thickness h to the trapdoor width B was 0.175. The reinforcement was laid at the bottom surface (represented by BS in Fig. 1) or/and at the top surface (represented by TS in Fig. 1) of the cushion in the tests with reinforcement. The total height of the backfill H was 256 mm, which was twice the trapdoor width B ($H = 2B$).

2.3 Reinforcement

Kraft paper with two different unit masses (i.e., 180 and 400 g/m2) was used as the reinforcement material in this study. Kraft paper with a unit mass of 180 g/m^2 (i.e., Reinforcement 1, R1) represented the reinforcement with lower stiffness while Kraft paper with a unit mass of 400 g/m^2 (i.e., Reinforcement 2, R2) represented the reinforcement with higher stiffness. Tensile tests were conducted on Kraft paper samples with a length of 200 mm and a width of 50 mm at an elongation rate of 10 mm/min, as shown in Fig. 2(a).

Fig. 2(b) shows the relationship between the tensile force and the global strain (i.e., the strain over the entire length of 200 mm) of the reinforcement. The reinforcement

Table 1 Test plan

Category	Test No.	Applied pressure p (kPa)	Reinforcement arrangement
Baseline (backfill self-weight)	T1	0	No reinforcement
	T2		A single R1 at BS
	T3		A single R2 at BS
	T4		Two R1 at BS and TS respectively
Static repetitive loading	ST1 (SR1)	8, 10, 12	No reinforcement
	ST2 (SR2)		A single R1 at BS
	ST3 (SR3)		A single R2 at BS
	ST4 (SR4)		Two R1 at BS and TS respectively
Cyclic loading	CT1 (CR1)	8, 10, 12	No reinforcement
	CT2 (CR2)		A single R1 at BS
	CT3 (CR3)		A single R2 at BS
	CT4 (CR4)		Two R1 at BS and TS respectively

Note: "T", "S", "C", and "R" in the column "Test No." stand for "trapdoor lowered", "static repetitive loading", "cyclic loading", and "referen ce test", respectively; Test No. within the brackets represents the corresponding reference test where no trapdoor displacement was mobilized; BS and TS represent the bottom and top surfaces of the aluminum cushion respectively

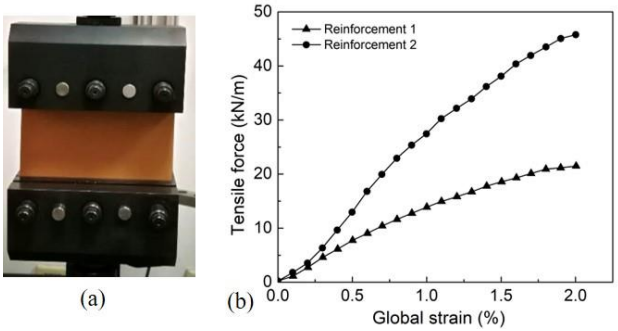

Fig. 2 Tensile tests conducted on Kraft paper: (a) photo of the tensile test and (b) tensile force and global strain curves of reinforcements R1 and R2

stiffness was determined as the secant slope of the tensile force–global strain curve at the corresponding reinforcement global strain. Specifically, the reinforcement stiffness at 2% global strain $J_{@2\%}$ were 1131 and 2236 kN/m for Reinforcement 1 (R1) and Reinforcement 2 (R2), respectively. Similarly, the reinforcement stiffness at 0.1% global strain $J_{@0.1\%}$ were 876 and 1562 kN/m for R1 and R2 respectively. Therefore, the average stiffness of R2 was approximately twice that of R1 (i.e., $J_{R2} \approx 2J_{R1}$).

2.4 Test plan

Table 1 provides the test plan used in this study. Four trapdoor tests (T1, T2, T3, and T4) under backfill self-weight with four different reinforcement arrangements were performed as baseline cases, which were (1) without reinforcement, (2) with a single R1 at the BS of the cushion, (3) with a single R2 at the BS of the cushion, and (4) with two R1 at the TS and BS of the cushion respectively.

The different reinforcement arrangements in T3 and T4 were intentionally designed by the authors to investigate potential advantages of using multiple low stiffness reinforcement layers placed at a certain distance in between as compared to using a single high stiffness reinforcement layer. For fair comparison, the total reinforcement stiffness of multiple "weak" reinforcement layers should be the same as that of a single "strong" reinforcement. Since the stiffness of R2 was approximately twice that of R1 (i.e., $J_{R2} \approx 2J_{R1}$), the total reinforcement stiffness values of T3 and T4 were approximately the same (i.e., $\Sigma J_{T3} \approx \Sigma J_{T4}$).

Four trapdoor tests under static repetitive loading (ST1, ST2, ST3, and ST4) and four trapdoor tests under cyclic loading (CT1, CT2, CT3, and CT4) were conducted to investigate the effects of localized surface loading on the development of soil arching considering the factors of loading magnitude and reinforcement arrangement. The reinforcement arrangements in the trapdoor tests under static repetitive and cyclic loading corresponded to those in the four baseline tests. Moreover, reference tests, as represented by the test number within the brackets in Table 1, were conducted to measure the average pressures acting on the trapdoor without any trapdoor displacement. In other words, there was no trapdoor displacement before and during loading in the reference tests. The measured average pressures in the references tests were used to represent $\gamma H+q$ in Eq. (3) in all the trapdoor tests, which will be discussed later in Section 2.5.

2.5 Calculation of average pressure and soil arching ratio

Considering the equilibrium of the reinforcement in the vertical direction as shown in Fig. 3, Eqs. (1) and (2) could be used to calculate the average pressures acting on the trapdoor (i.e., central trapdoor B4) and on the deflected reinforcement section above the trapdoor respectively. For tests without reinforcement, the average pressure acting on the trapdoor (σ_0) can be calculated using Eq. (1), as shown in Fig. 3(a)

$$\sigma_0 = \frac{F_t}{B \cdot d} \tag{1}$$

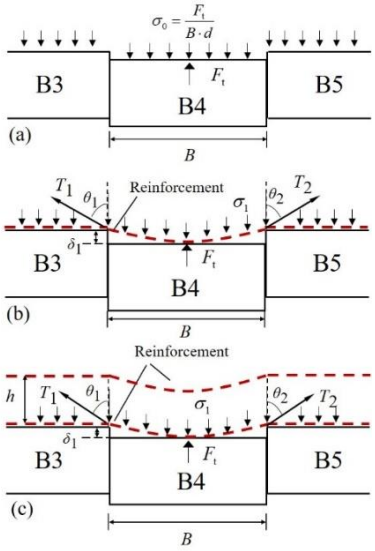

Fig. 3 Force diagram of the yielding portion: (a) without reinforcement, (b) with a single reinforcement layer, and (c) with two reinforcement layers

where B (m) = trapdoor width; d (m) = trapdoor thickness in the out-of-plane direction; F_t (kN) = the measured force acting on the trapdoor.

For tests with a single layer and with double layers of reinforcement, the average pressure acting on the deflected reinforcement section at the BS of the cushion (σ_1) can be calculated using Eq. (2), as shown in Figs. 3(b) and 3(c)

$$\sigma_1 B = T_1 \cos\theta_1 + T_2 \cos\theta_2 + \frac{F_t}{d} \tag{2}$$

where T_1 and T_2 (kN/m) = tensile forces at the left and right ends of the deflected reinforcement section respectively; θ_1 and θ_2 (◦) = angles of the left and right ends of the deflected reinforcement section above the central trapdoor with respect to the upward vertical direction respectively. The underlying assumption of Eq. (2) is that σ_1 was vertical and uniformly distributed. T_1 and T_2 were obtained by converting the global strains measured by the PIV technique to the tensile forces using the reinforcement stiffness calculated from the curves in Fig. 2(b). Under an ideal condition, T_1 should be equal to T_2. However, due to some local asymmetric distributions of the aluminum rods under both self-weight and localized loading, the global strains of the deflected reinforcement sections on the left and the right were not always equal, thus resulting in small differences between T_1 and T_2. For example, according to the PIV results, the global strains of the left and right deflected reinforcement sections were 0.12% and 0.11% respectively under an applied pressure of 8 kPa in ST2. As stated in Section 2.3, the reinforcement stiffness of R1 at 0.1% global strain was 876 kN/m. Therefore, the tensile forces T_1 and T_2 in R1 were T_1 = 0.12% × 876 = 1.05 kN/m and T_2 = 0.11% × 876 = 0.96 kN/m respectively. The difference between T_1 and T_2 was 0.09 kN/m, which was less than 10% of T_1 or T_2. θ_1 and θ_2 were manually measured from the photos taken during the tests. Due to the same reason as discussed above, θ_1 and θ_2 were not always equal. It should be noted that the differences between θ_1 and θ_2 were less than 5% according to the measured results.

To evaluate the degree of soil arching, soil arching ratio (SAR) was defined by McNulty (1965) as follows

$$\text{SAR} = \frac{\sigma_{v-b}}{\gamma H + q} \tag{3}$$

where $\sigma_{v\text{-}b}$ (kPa) = vertical pressure at the bottom of the yielding portion; γ (kN/m3) = unit weight of the backfill; H (m) = total height of the backfill; and q (kPa) = uniform surcharge applied on the backfill surface. SAR = 0 represents complete soil arching while SAR = 1 represents no soil arching. Al-Naddaf *et al.* (2019b) defined the soil arching ratio (SAR) above the reinforcement but the stress reduction ratio (SRR) below the reinforcement. When there is no reinforcement, SAR is equal to SRR. Similar to Al-Naddaf *et al.* (2019b), SAR was used in this study to evaluate the development of soil arching above reinforcement.

In the tests without reinforcement, $\sigma_{v\text{-}b}$ equaled to the average pressure acting on the trapdoor σ_0 shown in Fig. 3(a). In the tests with a single reinforcement layer, $\sigma_{v\text{-}b}$ equaled to the average pressure acting on the deflected reinforcement section σ_1 shown in Fig. 3(b). In the tests with two reinforcement layers, the average pressure acting on the deflected section of the lower reinforcement layer σ_1 shown in Fig. 3(c) was used as $\sigma_{v\text{-}b}$ to calculate the SAR for easy comparisons.

2.6 Test procedure

Before the placement of the aluminum rods and the reinforcement, the top surfaces of the seven hardwood blocks were adjusted to the same elevation by the control box to ensure that no soil arching existed before the trapdoor was lowered. After that, the load-transfer cushion and the reinforcement were laid on top of the blocks according to the test plan. The aluminum rods of different diameters were then placed in lifts of approximately 20 mm high until the height of the backfill H reached 256 mm. During the placement of the aluminum rods, the load applied onto each block was monitored to ensure a uniform density for the whole model.

In the baseline test without reinforcement, the trapdoor was lowered at two different speeds. First, the trapdoor was lowered by 10 increments of displacement (approximately 0.2 mm for each increment) until the trapdoor total displacement reached 2 mm. Second, the trapdoor was lowered by 23 increments (approximately 1.2 mm for each increment) until the trapdoor total displacement reached 29.6 mm. In the baseline tests with reinforcement, the trapdoor was lowered 40 times by approximately 0.2 mm at a time until the trapdoor total displacement reached approximately 8 mm. In all the baseline tests, a photo was taken each time after the trapdoor was lowered, which was used for the analysis of the backfill displacement field and the reinforcement deformation. In all the loading tests, the trapdoor was lowered in the same way as that in the baseline tests with reinforcement before localized surface loads were applied.

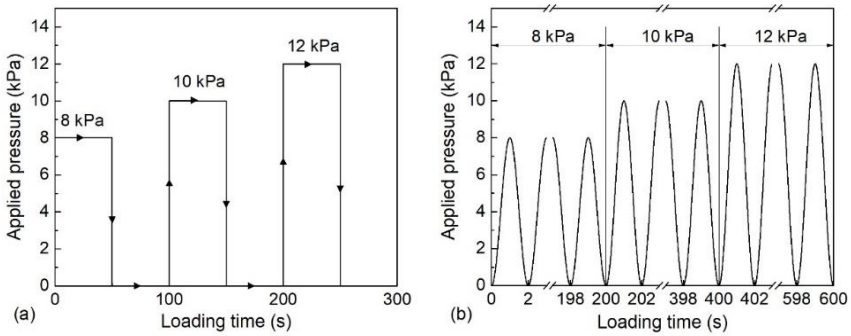

Fig. 4 Loading/unloading procedures for: (a) static repetitive loading and (b) cyclic loading

Fig. 4(a) shows the loading/unloading procedures for the tests under static repetitive loading: an 8-kPa pressure applied to the backfill surface for 50s followed by a photo taken, removed for 50s followed by another photo taken, then followed by next loading/unloading stage. The loading/unloading procedures under the applied pressures of 10 and 12 kPa were performed in the same way as that under the applied pressure of 8 kPa.

Fig. 4(b) presents three loading/unloading stages for the tests under cyclic loading with peak pressures of 8, 10, and 12 kPa. The same loading frequency of 0.5 Hz was used for all three stages. Each loading/unloading stage was applied in succession for 200 s. The loading wave form followed a sinusoid function since the sinusoid loading pattern is relatively simple and has been frequently used by researchers to investigate soil arcing under cyclic loading (e.g., Bhandari 2010, Han *et al*. 2015, Xu *et al.* 2019, Aqoub *et al.* 2020, Zhang *et al.* 2021a, b).

The loading values of each loading stage used in this study (i.e., 8 kPa, 10 kPa, 12 kPa) were determined based on the bearing capacity of the backfill under loading as well as the output consistency of the loading device. Based on the Terzaghi solution, the ultimate bearing capacity of the analogical soil under static loading can be calculated as $q_{ult} = 0.5\gamma \cdot L \cdot N_\gamma = 0.5 \times 22.4 \times 0.384 \times 9.3 \approx 40$ kPa where N_γ is a Terzaghi's bearing capacity factor associated with the contribution of the foundation width and is dependent on the friction angle of the backfill ϕ ($\phi = 25°$ in this study). A factor of safety FS = 3 was used to calculate the allowable pressure considering the effect of cyclic loading. Therefore, the maximum loading amplitude used in this study was determined as 12 kPa, which was slightly smaller than the allowable pressure $q_a = q_{ult}$ / FS = 13.3 kPa. The minimum loading amplitude used in this study, on the other hand, was determined based on the output consistency of the loading device. Although the loading device utilized an electric servo system with a force resolution of 1 N, the output forces under small loading amplitudes were not as consistent as those under relatively larger loading amplitudes. By conducting pre-tests, the authors found that, when the loading amplitude was equal or larger than 8 kPa, the consistency of the output forces satisfied the requirements of the trapdoor tests. Therefore, 8 kPa was determined as the minimum loading amplitude used in this study.

Video was taken during the tests under localized surface loading. The captured images of each loading/unloading stage were used for the subsequent analysis of the backfill displacement field and the reinforcement deformation using the PIV technique.

3. Test results

3.1 Baseline tests (under backfill self-weight)

The following discussion is about baseline trapdoor tests under backfill self-weight without localized surface loading. Fig. 5(a) shows the variations of the SARs with the normalized trapdoor displacements in T1 without reinforcement. The normalized trapdoor displacement is defined as the ratio of the trapdoor displacement to the trapdoor width. The evolution of soil arching had four stages: initial arching, maximum arching, stress recovery (or degradation of soil arching), and ultimate state, which is similar to those obtained by Chevalier *et al*. (2012), Iglesia *et al.* (2014), and Han *et al.* (2017). The ultimate state happened at approximately 10% normalized trapdoor displacement, which is in a good agreement with the value suggested by Han *et al*. (2017).

Figs. 5(b) and 5(c) show the variations of the SARs in T2 with a single R1 and in T3 with a single R2, respectively. For the baseline tests with reinforcement, the reinforcement separated from the trapdoor before the trapdoor displacement reached 8 mm. The vertical dash lines in Figs. 5(b) and 5(c) indicate the occurrence of the separation at the corresponding normalized trapdoor displacements that were approximately 2.50% and 2.03% for T2 and T3, respectively. In T2 with a single R1, the SAR decreased rapidly with the normalized displacement to the minimum value first, followed by an insignificant increase, and finally remained stable at the level close to the minimum value. This result indicates that the use of reinforcement limited or prevented stress recovery or degradation of soil arching. Similar conclusion was drawn by Shen *et al*. (2020) who investigated the global performance of geosynthetic-reinforced pile-supported embankments using centrifuge tests. In T3 with a single R2, stress recovery or degradation of soil arching barely happened. In addition, the stable value of the SARs in T3

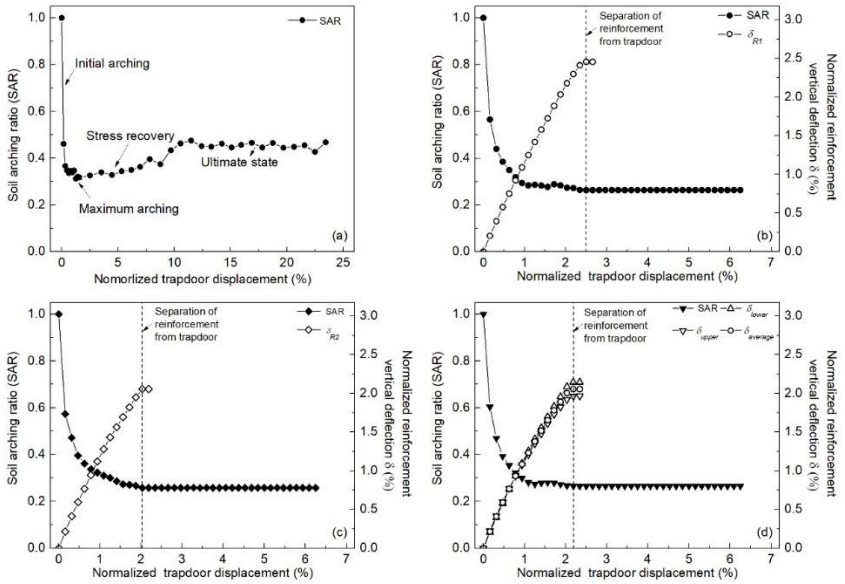

Fig. 5 Variations of SARs and maximum normalized reinforcement deflections with normalized trapdoor displacements in: (a) T1without reinforcement, (b) T2 with a single R1 at the BS of the cushion, (c) T3 with a single R2 at the BS of the cushion, and (d) T4 with two R1 at the BS and TS of the cushion respectively

with a single R2 was approximately the same as that in T2 with a single R1, demonstrating that reinforcement stiffness did not have a significant effect on the degree of soil arching under backfill self-weight. This is because that reinforcement was not well mobilized at small backfill displacements, thus resulting in similar shear stresses within the backfill. A similar result was obtained by van Eekelen *et al.* (2012). Figs. 5(b) and 5(c) also show the normalized maximum reinforcement vertical deflections (δ_{R1} and δ_{R2}) with the normalized trapdoor displacements in T2 with a single R1 and in T3 with a single R2, respectively. The normalized maximum reinforcement vertical deflection δ_R was defined as the ratio of the maximum reinforcement vertical deflection to the trapdoor width. Variations of δ_{R1} and δ_{R2} in Figs. 5(b) and 5(c) show that the high stiffness reinforcement resulted in less vertical deflection, which was expected and consistent with the conclusion drawn by van Eekelen *et al.* (2012).

Figs. 5(c) and (d) show the variations of the SARs in T3 with a single layer of R2 and in T4 with two layers of R1, respectively. The lower reinforcement layer at the BS of the cushion in T4 separated from the trapdoor at the normalized trapdoor displacement of 2.19%. Comparison of the results in Figs. 5(c) and 5(d) shows that the variations of the SARs in T3 with a single high stiffness R2 was similar to that in T4 with two low stiffness R1. The stable value of the SARs in T3 was approximately the same as that in T4. Fig.5(d) also shows the maximum normalized vertical deflections of the upper and lower R1 (δ_{upper} and δ_{lower}) with the normalized trapdoor displacements in T4. Comparison of the results in Figs. 5(c) and 5(d) shows that δ_{lower} was the largest one, δ_{upper} was the smallest one, and δ_{R2} was in between. The average normalized reinforcement deflection of the two R1 in T4 ($\delta_{average}$) was approximately the same as the normalized deflection of the single R2 (δ_{R2}) in T3. In conclusion, under backfill self-weight, no significant difference in the SARs and the reinforcement deflections existed between T3 with a single high stiffness R2 and T4 with two low stiffness R1 due to similar mobilized backfill displacements. In other words, under backfill self-weight, different reinforcement arrangements did not have a significant influence on the degree of soil arching and the reinforcement deflection when the total reinforcement stiffness were approximately the same (i.e., $\Sigma J_{T3} \approx \Sigma J_{T4}$).

3.2 Reference tests

The following discussion is about the reference tests under static repetitive and cyclic loading without trapdoor displacement. The purpose of reference tests was to decide $\gamma H+q$ in Eq. (3) when calculating the SARs for all the trapdoor tests under localized surface loading. Localized load p was applied to the backfill surface in this study, which was different from the uniform surcharge q considered in Eq. (3) by McNulty (1965). The localized surface load p distributes to a wider area with the depth while the uniform surcharge q remains approximately constant with the depth. Therefore, in this study, it was not reasonable to use q in the calculation of the SAR under localized surface loading. In all four reference tests under static repetitive loading (i.e., SR1 to SR4), the measured pressures on the central trapdoor (B4) increased dramatically at the beginning of each loading stage and quickly stabilized. Additionally, the differences of the measured pressures on the central trapdoor (B4) at the same loading/unloading stage between these four reference tests were less than 1%. Therefore, to save paper space, only the measured stable pressures on the central trapdoor (B4) in SR1, as shown in Table 2, were used to represent $\gamma H+q$ in Eq. (3) when calculating the SARs for all the trapdoor tests

Table 2 Measured pressures at different loading/unloading stages in the reference tests

Applied pressure (kPa)	SR1 (kPa)	CR1 (kPa)
0 (Initial)	5.79	5.75
8 (Load/Peak)	13.27	13.57
0 (Unload/Valley)	5.56	5.51
10 (Load/Peak)	15.35	15.13
0 (Unload/Valley)	5.56	5.56
12 (Load/Peak)	16.49	16.80
0 (Unload/Valley)	5.46	5.53

Notes: "Load" and "Unload" mean that a static pressure applied to the backfill and removed from the backfill respectively. "Peak" and "Valley" correspond to the applied peak and valley cyclic pressures respectively

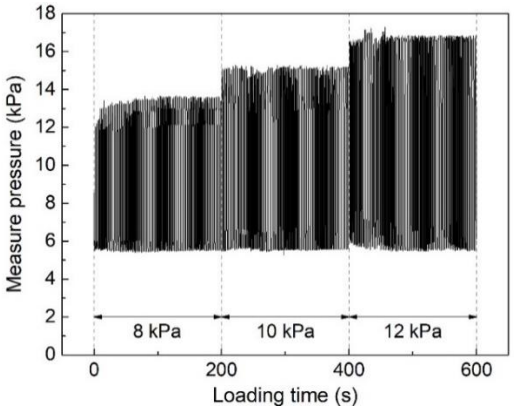

Fig. 6 Variations of the measured pressures on the central trapdoor (B4) with loading time in CR1

under static repetitive loading (i.e., ST1 to ST4). Similarly, the measured stable pressures on the central trapdoor (B4) in CR1, as shown in Table 2, were used to represent $\gamma H+q$ in Eq. (3) when calculating the SARs for all the trapdoor tests under cyclic loading (i.e., CT1 to CT4). "0 (initial)" in Table 2 represents the initial stage prior to surface loading after the backfill placement was finished.

Fig. 6 shows the variations of the measured pressures on the central trapdoor (B4) with loading time in CR1 including the results of three cyclic loading/unloading stages discussed previously in Section 2.6. The peak values in each cycle in Fig. 6 correspond to the peak magnitudes of the cyclic pressures (i.e., 8, 10, or 12 kPa) and the valley values in each cycle in Fig. 6 correspond to the valley pressures (i.e., 0 kPa). Fig. 6 also shows that the measured pressures had relatively large fluctuations in the peak and valley values at the beginning of each loading/unloading stage and then stabilized at the end. Taking the applied pressure of 8 kPa as an example, the measured peak and valley pressure values fluctuated within the ranges of 5.7 to 13.0 kPa and 6.1 to 5.6 kPa respectively at the beginning of the loading/unloading stage. After 10 seconds, the measured peak and valley pressure values were stabilized at approximately 13.4 and 5.7 kPa. Therefore, the average pressures in the last 50 seconds of each loading/unloading stage, as shown in Table 2, were used as $\gamma H+q$ in Eq. (3) in the calculation of the SARs for all the trapdoor tests under cyclic loading.

3.3 Trapdoor tests under static repetitive and cyclic loading

The following discussion is about trapdoor tests under localized surface loading (i.e., static repetitive and cyclic loading).

3.3.1 Maximum vertical deflections of reinforcement

Fig. 7 shows the maximum vertical deflections of the reinforcement at the center of the trapdoor B4 at different loading/unloading stages in the trapdoor tests under static repetitive and cyclic loadings. These maximum vertical deflections were determined at the last loading cycle of each loading/unloading stage. Legends "Load" and "Unload" in Fig. 7 mean that a static pressure applied to the backfill and removed from the backfill respectively. Legends "Peak" and "Valley" in Fig. 7 correspond to the applied peak and valley cyclic pressures respectively. In other words, legends "Load" and "Peak" represent the static repetitive and cyclic loading stages respectively while legends "Unload" and "Valley" represent the static repetitive and cyclic unloading stages respectively. It should be noted that the reinforcement vertical deflections were obtained from the captured photos analyzed by the PIV technique (White et al. 2003).

In all tests, an increase in the applied pressure produced an increase of the vertical deflection. Vertical deflections at the unloading stages were clearly smaller than those at the loading stages under both static repetitive and cyclic loads, suggesting that the reinforcement rebounded at the unloading stages but did not fully recover to the initial position (i.e., the vertical deflections at the applied pressure of 0 kPa). The differences of the vertical deflections between the loading and unloading stages increased gradually with the increase of the applied pressure. In addition, Fig. 7 clearly shows that the cyclic pressures induced larger vertical deflections than the static repetitive pressures at the same loading magnitude. However, the differences of vertical deflections between cyclic and static repetitive pressures decreased with the increase of the applied pressures.

The effects of reinforcement stiffness on the vertical deflection can be obtained by comparing the results in Figs. 7(a) and 7(b). Vertical defections of R1 were larger than

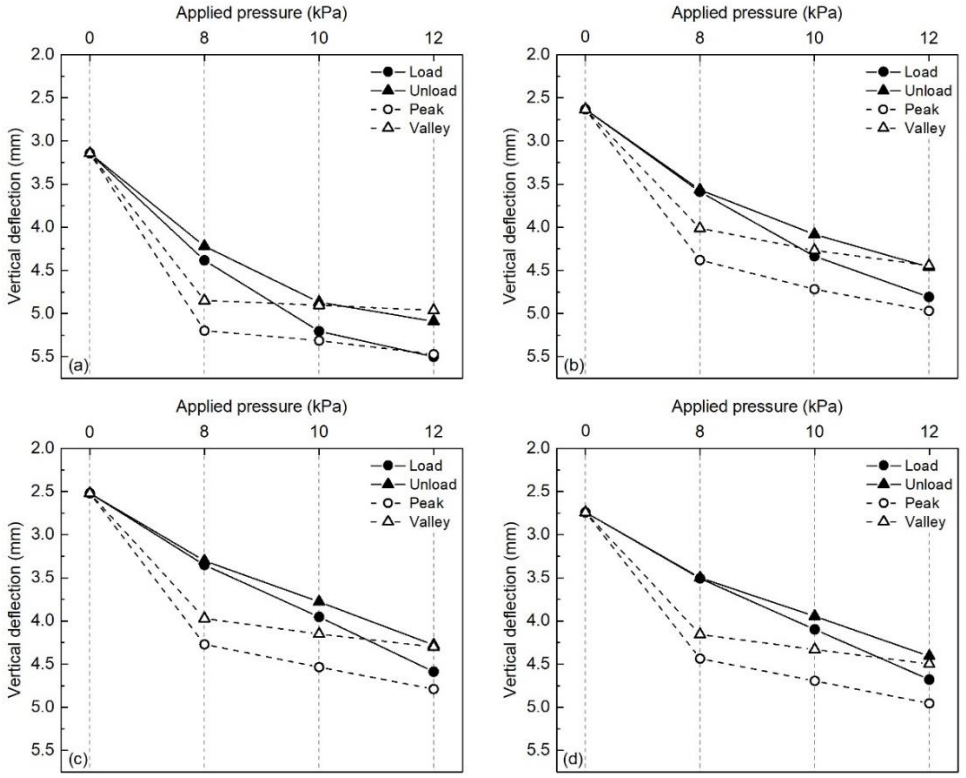

Note: Legends "Load" and "Unlond" mean a static pressure applied to and removed from the backfill, respectively.

Legends "Peak" and "Valley" correspond to the applied peak and valley cyclic pressures, repectively.

Fig. 7 Maximum vertical deflections of the reinforcement at the center of the trapdoor B4 in the trapdoor tests under static repetitive and cyclic loading: (a) R1 at the BS of the cushion in ST2/CT2, (b) R2 at the BS of the cushion in ST3/CT3, (c) upper R1 at the TS of the cushion in ST4/CT4, and (d) lower R1 at the BS of the cushion in ST4/CT4

those of R2 under backfill self-weight and under static repetitive and cyclic loading. This means that reinforcement stiffness had a large impact on the reinforcement vertical deflection under backfill self-weight and under localized surface loading. The effects of reinforcement arrangement on the vertical deflections can be obtained by comparing the results in Figs. 7(b)-7(d). Figs. 7(c) and 7(d) show the vertical defections of the upper and lower R1 in ST4/CT4, respectively. The vertical deflections of the upper R1 were always smaller than those of the lower R1. This result is consistent with the backfill deformation. The vertical deflections of the reinforcement in ST3/CT3 were similar to those in ST4/CT4 although the lower R1 in ST4/CT4 showed slightly smaller vertical deflections than those of the single R2 in ST3/CT3 at all the loading/unloading stages. Consequently, under static repetitive and cyclic loading, no significant difference in the reinforcement deflections existed between ST3/CT3 with a single high stiffness R2 and ST4/CT4 with two low stiffness R1 when the total reinforcement stiffness of ST3/CT3 and ST4/CT4 were approximately the same (i.e., $\Sigma J_{T3} \approx \Sigma J_{T4}$).

3.3.2 Tensile forces of reinforcement

It should be noted that the reinforcement tensile forces discussed in this section were calculated as the products of the reinforcement stiffness at 0.1% global strain $J_{@0.1\%}$ and the global strains measured by the PIV technique. The reason of using $J_{@0.1\%}$ to calculate the tensile forces was that the measured maximum global strain was 0.09% in R1 at the applied cyclic peak pressure of 12 kPa, which was slightly smaller than 0.1%.

Fig. 8 shows the tensile forces of the reinforcement in ST2/CT2, ST3/CT3, and ST4/CT4, respectively. Legends in Fig. 8 have the same meaning as those in Fig. 7. These tensile forces were determined based on the reinforcement tensile forces at the last loading cycle of each loading/unloading stage. An obvious increment in the tensile forces was noticed when the localized surface loading was applied. It can also be observed that the tensile forces increased gradually with the increase of the applied pressures at all the loading/unloading stages. Tensile forces at the loading stages increased at a faster rate than those at the unloading stages.

The effects of the reinforcement stiffness on the reinforcement tensile forces can be obtained by comparing the results in Figs. 8(a) and 8(b). It can be found that the tensile forces of R2 in ST3/CT3 were slightly larger than those of R1 in ST2/CT2 at the static repetitive and cyclic loading stages while the tensile forces of R1 in ST2/CT2 and R2 in ST3/CT3 were approximately the same at the static repetitive and cyclic unloading stages. The high stiffness reinforcement resulted in smaller vertical

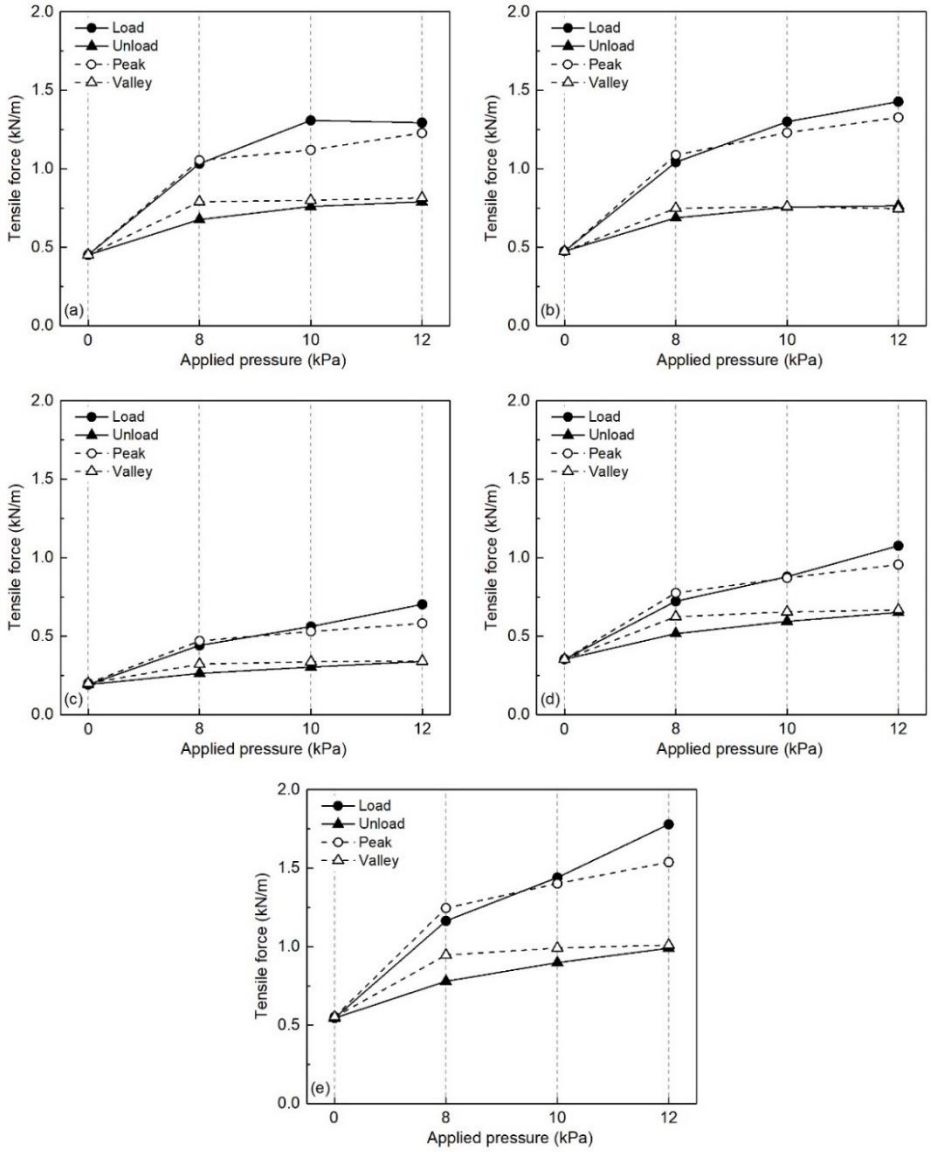

Note: Legends "Load" and "Unlond" mean a static pressure applied to and removed from the backfill, respectively.

Legends "Peak" and "Valley" correspond to the applied peak and valley cyclic pressures, repectively.

Fig. 8 Variations of tensile forces of reinforcement: (a) R1 at the BS of the cushion in ST2/CT2, (b) R2 at the BS of the cushion in ST3/CT3, (c) upper R1 at the TS of the cushion in ST4/CT4, (d) lower R1 at the BS of the cushion in ST4/CT4, and (e) sum of upper and lower R1 in ST4/CT4

deflections, as shown in Fig. 7, but slightly higher tensile forces at the loading stages.

The effects of reinforcement arrangement on the reinforcement tensile forces can be obtained by comparing the results in Figs. 8(b)-8(e). Figs. 8(c) and 8(d) show that the tensile forces of the upper R1 were smaller than those of the lower R1, suggesting that two layers of reinforcement had different tensile forces. Comparing the results in Figs. 8(b)-8(d) show that the tensile forces of both the upper and lower R1 in ST4/CT4 were smaller those of R2 in ST3/CT3. Fig. 8(e) shows the sum of the tensile forces of the upper and lower R1 in ST4/CT4. Figs. 8(b) and 8(e) indicate that the sum of the tensile forces of the upper and lower R1 in ST4/CT4 was larger than the tensile forces of R2 in ST3/CT3 at different loading/unloading stages.

These results suggest that the use of two low stiffness R1 in ST4/CT4 mobilized more tensile forces of the reinforcement than the use of a single high stiffness R2 in ST3/CT3 when the total reinforcement stiffness values of ST3/CT3 and ST4/CT4 were approximately the same (i.e., $\Sigma J_{T3} \approx \Sigma J_{T4}$).

3.3.3 SARs and stress redistribution

Fig. 9 shows the variations of the peak and valley values of the average pressures acting on the trapdoor (σ_0) and on the deflected reinforcement section (σ_1) under each loading/unloading cycle in CT1, CT2, CT3, and CT4. It should be noted that σ_0 and σ_1 were calculated using Eqs. (1) and (2) respectively. Fig. 9 also shows three obvious stages corresponding to the three loading/unloading stages

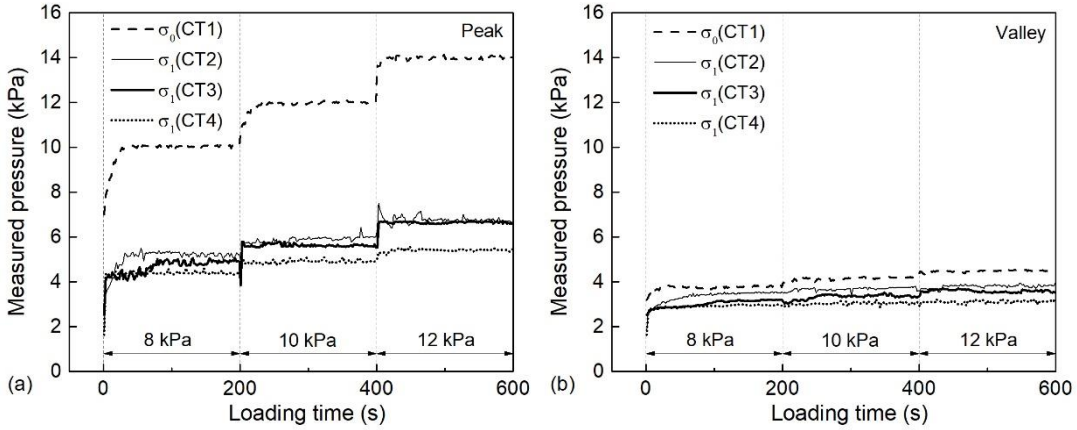

Fig. 9 Variations of average pressures acting on the trapdoor and on the deflected reinforcement section in each loading/unloading cycle in the trapdoor tests under cyclic loading: (a) peak values and (b) valley values

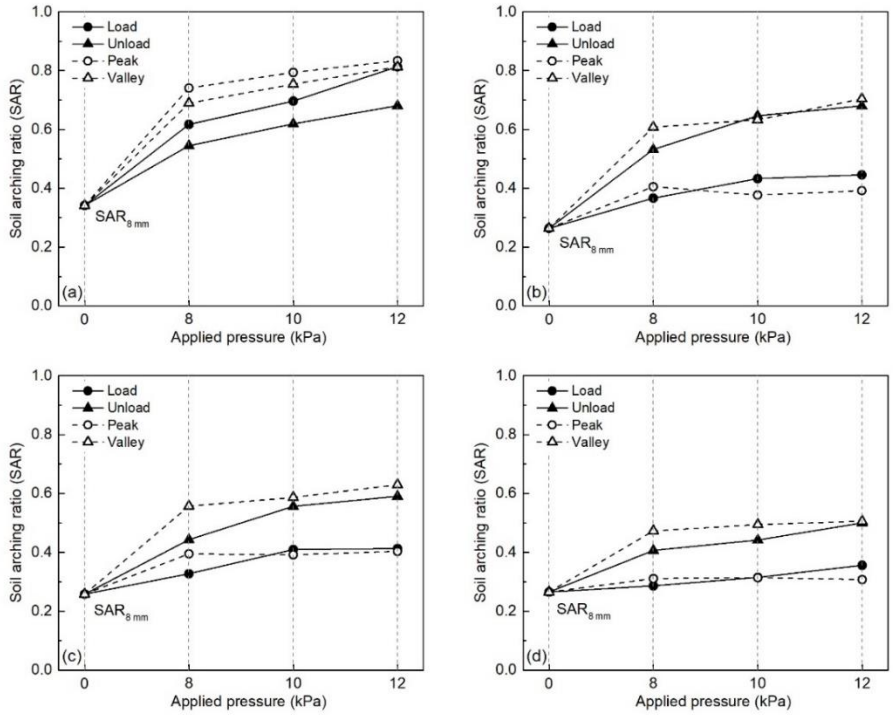

Note: Legends "Load" and "Unlond" mean a static pressure applied to and removed from the backfill, respectively.
Legends "Peak" and "Valley" correspond to the applied peak and valley cyclic pressures, repectively.

Fig. 10 Variations of the SARs in trapdoor tests under static repetitive and cyclic loading: (a) ST1/CT1, (b) ST2/CT2, (c) ST3/CT3, and (d) ST4/CT4

discussed previously in Section 2.6. At each loading/unloading stage, the measured pressures increased dramatically at the beginning and then gradually reached a stable value with the loading time. This pressure increase at the beginning was due to the increased applied load. With the increase of the loading time, there was a gradual stress adjustment due to soil arching degradation until reaching new equilibrium. It should be noted that, in the trapdoor tests under cyclic loading, the average measured pressures in the last 50 seconds of each loading/unloading stage were used as $\sigma_{v\text{-}b}$ in Eq. (3) to calculate the SAR.

Fig. 10 shows the variations of the SARs in the trapdoor tests after the 8 mm trapdoor displacement prior to applying localized surface loads ($SAR_{8\ mm}$), at the static repetitive loading and unloading stages respectively (SAR_{load} and SAR_{unload}), and at the cyclic loading and unloading stages respectively (SAR_{peak} and SAR_{valley}). Fig. 10(a) shows the variations of the SARs in ST1/CT1 for the trapdoor tests without reinforcement. It is obvious that the SARs within the static repetitive and cyclic loading/unloading stages were higher than those after the 8 mm trapdoor displacement $SAR_{8\ mm}$, indicating that both static repetitive

and cyclic loading caused negative effects on soil arching when no reinforcement was utilized. The SARs increased with the increase of the loading magnitudes. More importantly, under static repetitive loading, the SARs within the loading stages SAR_{load} were greater than those within the unloading stages SAR_{unload}. Similar results of the SARs could be observed under cyclic loading (i.e., $SAR_{peak} > SAR_{valley}$). These results indicate that, for trapdoor tests without reinforcement, soil arching degraded at the loading stages and partly recovered at the unloading stages.

For the trapdoor tests with reinforcement, Figs. 10(b)-(d) show the variations of the SARs in ST2/CT2 with a single R1, ST3/CT3 with a single R2, and ST4/CT4 with two R1, respectively. The SARs within the static repetitive and cyclic loading stages (i.e., SAR_{load} and SAR_{peak}) in the trapdoor tests with reinforcement (i.e., ST2/CT2, ST3/CT3, and ST4/CT4) were smaller than those in the trapdoor tests without reinforcement (i.e., ST1/CT1), indicating that the use of reinforcement minimized the degradation of soil arching under localized surface loading. Within both static repetitive and cyclic loading stages, SAR_{load} and SAR_{peak} increased generally with the increase of the applied pressures, demonstrating that the degradation of soil arching became more significant with the increase of the loading magnitudes. In the trapdoor tests with reinforcement (i.e., ST2, ST3, and ST4), the SARs within the static repetitive loading stages SAR_{load} were smaller than those within the static repetitive unloading stages SAR_{unload}, which are different from the results in the trapdoor tests without reinforcement (i.e., ST1). Similarly, the SARs within the cyclic loading stages SAR_{peak} were smaller than those within the cyclic unloading stages SAR_{valley} in the trapdoor tests with reinforcement (i.e., CT2, CT3, and CT4), which are different from the results in the trapdoor tests without reinforcement (i.e., CT1). After the localized surface load was removed, the backfill above the trapdoor (i.e., the yielding portion) and the stationary portion rebounded. Since the reinforcement was laid at the BS of the cushion, the rebound of the backfill above the trapdoor was controlled by the rebound of the reinforcement during unloading. The rebound of the reinforcement, as shown in Fig. 7, was larger than the rebound of the backfill above the stationary part measured by the PIV technique. As a result, during unloading, the reinforcement applied the load to the backfill above the reinforcement and the relative displacement between the backfill above the trapdoor and the stationary portion decreased. Therefore, as compared to the results within the static repetitive and cyclic loading stages, soil arching degraded at the static repetitive and cyclic unloading stages when reinforcements were utilized.

The effects of the reinforcement stiffness on the SARs can be obtained by comparing the results in Figs. 10(b) and 10(c). In general, the SARs in ST2/CT2 were slightly larger than those in ST3/CT3. These results suggest that the high stiffness reinforcement had the advantages of minimizing soil arching degradation. Since the differences of the tensile forces in R1 and R2 were not significant as shown in Figs. 8(a) and 8(b), the average pressures on the deflected reinforcement section (σ_1) were mainly dominated by the reinforcement rotation angle θ as shown in Fig. 3. The high stiffness reinforcement resulted in smaller vertical deflections as shown in Figs. 7(a) and 7(b) and therefore larger θ. According to Eq. (2), the increase of θ reduced the vertical component of the tensile force in the reinforcement, thus resulting in lower σ_1 and consequently smaller SARs.

The effects of reinforcement arrangement on the SARs can be obtained by comparing the results in Figs. 10(c) and 10(d). It can be found that the SARs in ST4/CT4 with two R1 were significantly smaller than those in ST3/CT3 with a single R2. The tension developed in the upper R1 in ST4/CT4 as shown in Fig. 8(c), thus reducing the vertical pressures acting in the lower R1. In other words, as compared to the use of a single stiffer R2 at the BS of the cushion, the use of two layers of low stiffness R1 at the TS and BS of the cushion respectively promoted the tensioned membrane effect of the upper reinforcement and therefore minimized soil arching degradation under localized surface loading and unloading when the total reinforcement stiffness values were approximately the same (i.e., $\Sigma J_{T3} \approx \Sigma J_{T4}$).

4. Comparison with analytical solutions

This section discusses the results of the trapdoor tests under both backfill self-weight (i.e., baseline tests) and localized surface loading (i.e., static repetitive and cyclic loading) as compared to the analytical multi-stage soil arching model proposed by Iglesia *et al*. (2014) for estimating average vertical pressures acting on the trapdoor or on the deflected reinforcement section.

As compared to strain and stress contours, displacement contours of backfill have been more commonly used by researchers to reveal different soil arching developments (e.g., Lai *et al.* 2020, Rui *et al*. 2016b, 2019, 2020, Zhang *et al.* 2021a, b, Xu *et al*. 2019, Bi *et al*. 2020, Zhao *et al.* 2021). For example, by analyzing displacement contours under different conditions, Rui *et al.* (2016a, 2016b, 2019) proposed three soil arching evolution patterns (i.e., triangular expanding pattern, tower-shaped evolution pattern, and equal settlement pattern) from unreinforced trapdoor tests and two soil arching evolution patterns (i.e., concentric ellipse pattern and equal settlement pattern-concentric arches) from reinforced trapdoor tests. Zhang *et al.* (2021a, b) also utilized displacement contours to investigate the degradation of soil arching under localized surface loading and concluded that the degradation of soil arching first happened locally at the center above the trapdoor. Bi *et al.* (2020) identified two types of soil arching evolution under cyclic loading, namely stable cases and collapse cases. Therefore, this study also used displacement contours of the backfill to identify developments of soil arching. Fig. 11 shows the displacement contours of the backfill in baseline trapdoor tests T1 and T4 under the backfill self-weight without and with reinforcement respectively. Fig. 11(a) shows that, for the baseline trapdoor test without reinforcement (i.e., T1), vertical slip surfaces above the central trapdoor B4 developed in the backfill and extended to the backfill surface. On the other hand, Fig. 11(b) shows that, for the baseline trapdoor test with

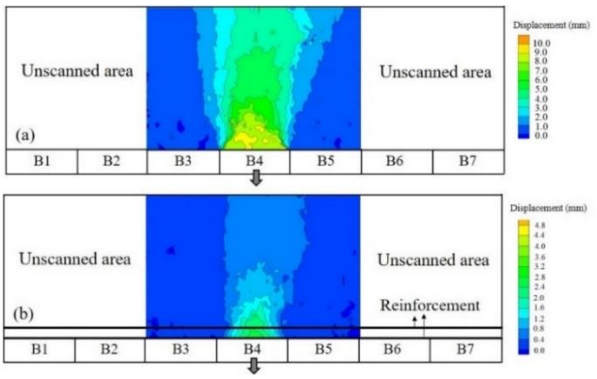

Fig. 11 Displacement contours of the backfill under backfill self-weight in baseline trapdoor tests: (a) T1 at the normalized trapdoor displacement of 10%, and (b) T4 at the normalized trapdoor displacement of 6.25%

reinforcement (i.e., T4), the deformation of the backfill concentrated within the triangular region above the deflected reinforcement section and the use of the reinforcement at the bottom of the backfill restrained the slip surfaces from extending to the surface. Iglesia *et al.* (2014) proposed using physical arches to describe the soil arching phenomenon in trapdoor tests. With the increase of the trapdoor displacement, the shape of the physical arch was initially curved (minimum load), then evolved to a triangular configuration (intermediate state), and finally transformed into a prism with a rectangular cross-section (terminal state). The terminal state with the vertical slip surfaces is the same as that proposed by Terzaghi (1943). According to Fig. 11(a), the stage of soil arching without reinforcement at the normalized trapdoor displacement of 10% was consistent with the terminal state with a rectangular arch proposed by Terzaghi (1943) and Iglesia *et al.* (2014). This finding was also confirmed by Han *et al.* (2017) in their studies of progressive development of 2D soil arching with displacement. For the development of soil arching with reinforcement, the use of reinforcement limited soil displacement at the bottom so that stress recovery or degradation of soil arching was minimized or prevented. According to Fig. 11(b), the stage of soil arching with reinforcement at the normalized trapdoor displacement of 6.25% was consistent with the intermediate state with a triangular arch proposed by Iglesia *et al*. (2014).

Table 3 shows the SARs under the backfill self-weight ($SAR_{s\text{-}w}$) from the baseline test results and calculated by the analytical multi-stage soil arching model proposed by Iglesia *et al*. (2014). The lateral earth pressure coefficient K was required as one of the parameters for calculation when using the analytical multi-stage soil arching model proposed by Iglesia *et al*. (2014). Three different K were used in the calculations, which were the Rankine active lateral earth pressure coefficient, $K_a = (1 - \sin\phi)/(1 + \sin\phi) = 0.41$, the coefficient suggested by Terzaghi (1943), $K_T = 1$, and the Rankine passive lateral earth pressure coefficient, $K_p = (1 + \sin\phi)/(1 - \sin\phi) = 2.46$.

For the baseline trapdoor test without reinforcement (i.e., T1), the rectangular arch model proposed by Iglesia *et al.* (2014) was used to calculate the average vertical pressure acting on the trapdoor under the backfill self-weight. By adopting the boundary condition of zero pressure at the top of the backfill surface, the rectangular arch model was simplified into Eq. (4). It should be noted that Eq. (4) was essentially the same as the soil arching model proposed by Terzaghi (1943) when the lateral earth pressure coefficient K is assumed to be K_T

$$\sigma_{v\text{-}b} = \frac{B \cdot \gamma}{2K \cdot \tan\phi} \cdot \left(1 - e^{-H \cdot \frac{2K \cdot \tan\phi}{B}}\right) \tag{4}$$

where B (m) = trapdoor width (B = 0.128 m in this study); γ (kN/m^3) = unit weight of the backfill (γ = 22.4 kN/m^3); K = lateral earth pressure coefficient; ϕ (°) = friction angle of the backfill (ϕ = 25° in this study); H (m) = backfill height ($H = 2B$ = 0.256 m). Table 3 shows that the use of K_T in Eq. (4) gave an accurate prediction of the $SAR_{s\text{-}w}$ at the ultimate state while K_a and K_p overestimated and underestimated the $SAR_{s\text{-}w}$ at the maximum arching and ultimate states respectively.

The triangular arch model proposed by Iglesia et al. (2014) was used to calculate the $SAR_{s\text{-}w}$ for the baseline trapdoor tests with reinforcement under the backfill self-weight (i.e., T2, T3, and T4). Based on the triangular arch model, the average vertical pressure acting on the deflected reinforcement section can be calculated using Eq. (5) with different lateral earth pressure coefficients K

$$\sigma_{v\text{-}b} = \gamma \cdot B \cdot \left(\frac{H \cdot K}{4H \cdot \cot\phi} + \frac{\cot\phi}{4}\right) \tag{5}$$

Table 3 shows that all the reinforced trapdoor tests had the same $SAR_{s\text{-}w}$ at the maximum arching and ultimate states based on the baseline test results, which were consistent with the previous findings in Section 3.1 that stress recovery or degradation of soil arching did not exist in the reinforced trapdoor tests under the backfill self-weight. Table 3 also shows that the calculated results using Eq. (5) and K_a were in good agreement with the test results while the use of K_T and K_p obviously overestimated the $SAR_{s\text{-}w}$.

In summary, Table 3 shows that, to get better agreement with the baseline test results, different lateral earth pressure coefficients K should be used in the calculation of $\sigma_{v\text{-}b}$ for soil arching without reinforcement (i.e., T1) and with reinforcement (i.e., T2 to T4). This is because that soil arching without and with reinforcement corresponded to different stages of soil arching described by the analytical multi-stage soil arching models proposed by Iglesia *et al.* (2014). Different stages of soil arching happened at different backfill displacements. Since K is also a displacement-dependent parameter, it is reasonable to use different values of K for the analytical multi-stage soil arching models proposed by Iglesia *et al.* (2014). Table 3 indicates that K_T gave the best agreement with the results of T1 (i.e., the terminal state of soil arching with large backfill displacements) while K_a gave the best agreement with the results of T2 to T3 (i.e., the intermediate state of soil arching with small backfill displacements). These conclusions from Table 3 are deemed reasonable since K_T is larger than K_a.

Table 3 Soil arching ratios under the backfill self-weight ($SAR_{s\text{-}w}$) from the baseline test results and calculated using the analytical multi-stage soil arching model proposed by Iglesia *et al*. (2014)

Test No.	$SAR_{s\text{-}w}$ from baseline test results		$SAR_{s\text{-}w}$ based on the analytical soil arching model*		
	Maximum arching	Ultimate state	Using K_a	Using K_T	Using K_p
T1	0.312	0.463	0.701	0.453	0.215
T2	0.263	0.263	0.291	0.323	0.394
T3	0.266	0.266	0.291	0.323	0.394
T4	0.265	0.265	0.291	0.323	0.394

Note: *The analytical soil arching models at the terminal state with a rectangular arch and at the intermediate state with a triangular arch proposed by Iglesia et al. (2014) were used to calculate $SAR_{s\text{-}w}$ for the baseline trapdoor tests under the backfill self-weight without reinforcement (i.e., T1) and with reinforcement (i.e., T2 to T4) respectively

Under both the backfill self-weight and localized surface loading, the average vertical pressure acting on the central trapdoor B4 or on the deflected reinforcement section (i.e., at the bottom of the yielding portion z = 0) can be calculated using the following equation

$$\sigma_{v-b} = \gamma \cdot H \cdot \mathrm{SAR}_{\text{s-w}} + \Delta p \cdot \mathrm{SAR}_{\text{load/peak}} \quad (6)$$

where Δp (kPa) = additional average vertical pressure induced by localized surface loading at the bottom of the yielding portion without considering the soil arching effect; $SAR_{load/peak}$ = soil arching ratio at the static repetitive or cyclic loading stages; $SAR_{s\text{-}w}$ = soil arching ratio under the backfill self-weight. Assuming that the SAR under the backfill self-weight $SAR_{s\text{-}w}$ is the same as that under localized surface loading $SAR_{load/peak}$, Eq. (6) can be simplified into

$$\sigma_{v-b} = \left(\gamma \cdot H + \Delta p\right) \cdot \mathrm{SAR}_{\text{s-w}} \quad (7)$$

Wang and Chen (2019) utilized a similar assumption (i.e., same load transfer efficacy under the backfill self-weight and under loading) to calculate the additional vertical pressure induced by a footing load applied at the backfill surface. According to the baseline trapdoor test results in Table 3, for the trapdoor tests without reinforcement (i.e., ST1 and CT1), the calculated $SAR_{s\text{-}w}$ = 0.453 based on the rectangular arch model proposed by Iglesia *et al*. (2014) and K_T = 1 were used to calculate the average vertical pressure acting on the central trapdoor B4 under both the backfill self-weight and localized surface loading. For the trapdoor tests with reinforcement (i.e., ST2 to ST4 and CT2 to CT4), on the other hand, the calculated $SAR_{s\text{-}w}$ = 0.291 based on the triangular arch model proposed by Iglesia *et al*. (2014) and K_a = 0.41 were utilized to calculate the average vertical pressure acting on the deflected reinforcement section under both the backfill self-weight and localized surface loading. Two different stress distribution methods (i.e., the Boussinesq solution and the 2 to 1 distribution method) were used to calculate the Δp in Eq. (7) as did by Al-Naddaf *et al*. (2019a).

Fig. 12 shows the comparison of the test results with the calculated average vertical pressures on the central trapdoor B4 or on the deflected reinforcement section under both the backfill self-weight and localized surface loading using Eq. (7). For the trapdoor tests without reinforcement (i.e., ST1 and CT1), Figs. 12(a) and 12(b) show that Eq. (7) with the additional average vertical pressure calculated by both the Boussinesq solution and the 2 to 1 distribution method greatly underestimated the average pressures on the central trapdoor B4. In addition, Fig. 12(a) and 12(b) show the calculated vertical pressures using the Boussinesq solution and the 2 to 1 distribution method without considering the soil arching effect (i.e., substituting $SAR_{s\text{-}w}$ = 1.0 into Eq. (7) led to $\sigma_{v\text{-}b} = (\gamma H + \Delta p) \cdot 1 = \gamma H + \Delta p$). Figs. 12(a) and 12(b) show that Eq. (7) without considering the soil arching effect gave reasonable predictions of the average pressures on the central trapdoor under both the backfill self-weight and localized surface loading. In other words, for the trapdoor tests without reinforcement, soil arching fully degraded (i.e., collapsed) under localized surface loading, especially at a larger applied load, and consequently failed to transfer the applied load from the yielding portion to the stationary portions. Zhang *et al*. (2021b) observed similar results in their multiple trapdoor tests after global degradation of soil arching.

For the trapdoor tests with reinforcement (i.e., ST2 to ST4 and CT2 to CT4), on the other hand, Figs. 12(c) and 12(d) show that the calculated pressures without considering the soil arching effect significantly overestimated the average pressures on the deflected reinforcement section under both the backfill self-weight and localized surface loading. In other words, the use of reinforcement prevented partly the degradation of soil arching under localized surface loading, which was consistent with the previous findings in Section 3.3. Figs. 12(c) and 12(d) also show that the calculated pressures considering the soil arching effect slightly underestimated the average pressures on the deflected reinforcement under both the backfill self-weight and localized surface loading. Under localized loading, the applicability of the triangular arch model as well as the use of K_a might be questionable thus requiring further research.

5. Limitations

Even though this study was carefully planned and conducted, there are still some limitations. When localized loading was applied to the backfill surface in the trapdoor

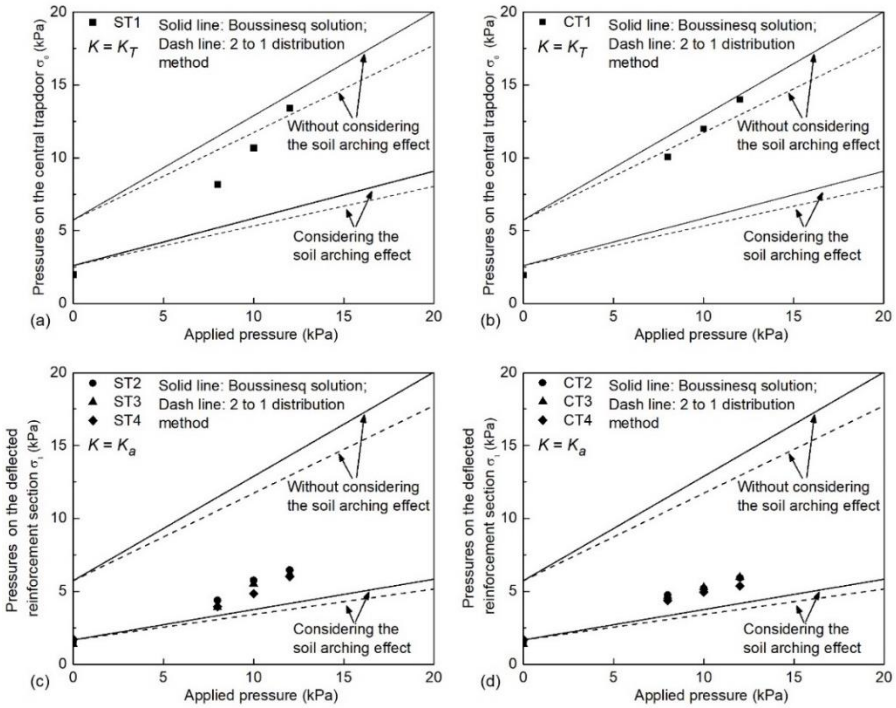

Fig. 12 Comparison of the test results with the calculated vertical pressures on the central trapdoor B4 or on the deflected reinforcement section under both the backfill self-weight and localized surface loading in: (a) ST1, (b) CT1, (c) ST2 to ST4, and (d) CT2 to CT4

tests with reinforcement, the reinforcement was already separated from the trapdoor. Therefore, the findings from the trapdoor tests with reinforcement are more applicable to the field applications using geotextile reinforcement to bridge over localized voids. However, the theoretical analyses of soil arching development presented in Section 4 demonstrate that this study still gave valuable insights to the understanding of soil arching development with and without reinforcement under localized surface loading and these limitations would not affect the main conclusions of this study.

6. Conclusions

This paper presents twelve plane-strain trapdoor tests utilizing a trapdoor test box to investigate the effects of reinforcement on the development of soil arching under backfill self-weight and localized surface loading (i.e. static repetitive and cyclic loading) with a loading plate width three times the trapdoor width. An analogical soil made of aluminum rods with three different diameters was used as the backfill and Kraft paper with two different stiffness values was used as the reinforcement material in this study. Four different cases of reinforcement arrangements were used: (1) no reinforcement, (2) a single layer of low stiffness reinforcement R1, (3) a single layer of high stiffness reinforcement R2, and (4) two layers of low stiffness reinforcement R1 with a backfill of certain thickness in between (i.e., cushion). The stiffness of reinforcement R2 was approximately twice the stiffness of reinforcement R1, thus resulting in the same total reinforcement stiffness for Case (3) and Case (4). The following conclusions can be drawn from this study:

- Under backfill self-weight without localized surface loading, reinforcement minimized or prevented degradation of soil arching. Both static repetitive and cyclic localized surface loading resulted in degradation of soil arching regardless of whether reinforcement was used or not. Soil arching without reinforcement recovered partly during the static repetitive and cyclic unloading stages. Soil arching with reinforcement, however, degraded more during the static repetitive and cyclic unloading stages as compared to the results during the static repetitive and cyclic loading stages.
- Under backfill self-weight without localized surface loading, different reinforcement stiffness did not have a significant effect on the degree of soil arching. Under static repetitive and cyclic loading, the high stiffness reinforcement had the advantages of more effectively reducing reinforcement deflections and minimizing degradation of soil arching than the low stiffness reinforcement.
- Under backfill self-weight without localized surface loading, different reinforcement arrangements did not have a significant influence on the degree of soil arching and the reinforcement deflections when the total reinforcement stiffness were approximately the same. Under static repetitive and cyclic loading, two low stiffness reinforcement layers mobilized more total tensile forces than a single high stiffness reinforcement. Consequently, as compared to a single high stiffness reinforcement, two low stiffness reinforcement layers with a backfill of certain

thickness in between promoted the tensioned membrane effect of the upper reinforcement and minimized the soil arching degradation under localized surface loading when their total reinforcement stiffness were approximately the same. It should be pointed out that this finding is based on the ratio of the cushion thickness h to the trapdoor width B of 0.175. An increase or decrease of this ratio may change the outcome, which should be further verified in future studies.

• Due to different states of soil arching developing with and without reinforcement, the analytical multi-stage soil arching model proposed by Iglesia *et al*. (2014) was selected in this study to calculate the average vertical pressures acting on the trapdoor or on the deflected reinforcement under both the backfill self-weight and localized surface loading. This study assumed that the soil arching ratio under the backfill self-weight was the same as that under localized surface loading. The comparison between the calculated and test results shows that, for the trapdoor tests without reinforcement, soil arching mostly degraded or collapsed under localized surface loading so that no soil arching should be considered in the calculation of the vertical pressures for safety. For the trapdoor tests with reinforcement, the calculated results considering the soil arching effect served as lower boundaries for the average pressures on the deflected reinforcement section.

The above conclusions were made based on the condition that the backfill height was twice the trapdoor width. An increase of the backfill height may influence the effect of localized surface loading on soil arching and these conclusions, thus requiring further studies.

Acknowledgements

The results presented in this paper are part of the research projects (No. 51478349 & No. 41272293) sponsored by the National Natural Science Foundation of China. This financial support is greatly appreciated.

References

Al-Naddaf, M., Han, J., Jawad, S., Abdulrasool, G. and Xu, C. (2017), "Investigation of stability of soil arching under surface loading using trapdoor model tests", *Proceedings of the 19th International Conference on Soil Mechanics and Geotechnical Engineering*, Korea, September.

Al-Naddaf, M., Han, J., Xu, C., Jawad, S. and Abdulrasool, G. (2019b), "Experimental investigation of Soil Arching Mobilization and Degradation under localized surface loading", *J. Geotech. Geoenviron. Eng.*, **145**(12), 04019114. https://doi.org/10.1061/(ASCE)GT.1943-5606.0002190.

Al-Naddaf, M., Han, J., Xu, C. and Rahmaninezhad, M.S. (2019a), "Effect of geofoam on vertical stress distribution on buried structures subjected to static and cyclic footing loads", *J. Pipel. Syst. Eng. Pract.*, **10**(1), 04018027. https://doi.org/10.1061/(ASCE)PS.1949-1204.0000355.

Aqoub, K., Mohamed, M. and Sheehan, T. (2020), "Analysis of unreinforced and reinforced shallow piled embankments under cyclic loading", *Geosynth. Int.*, **27**(2), 182-199. https://doi.org/10.1680/jgein.19.00010.

Balaban, E. and Onur, M.I. (2018), "Comparison of behaviour of basal reinforced piled embankment with two layer of reinforcement", *Geomech. Eng.*, **16**(3), 233-245. https://doi.org/10.12989/gae.2018.16.3.233.

Bao, N., Wei, J., Chen, J.F. and Stephen, A. (2021), "Investigation of soil arching under cyclic loading using the discrete element method", *Int. J. Geomech.*, **21**, 04021117. https://doi.org/10.1061/(ASCE)GM.1943-5622.0002090.

Bhandari, A. (2010), "Micromechanical analysis of geosynthetic-soil interaction under cyclic loading", Ph.D. Dissertation; the University of Kansas, KS, USA.

Bhandari, A. and Han, J. (2018), "Two-dimensional physical modelling of soil displacements above trapdoors", *Geotech. Res.*, **5**(2), 68-80. https://doi.org/10.1680/jgere.18.00002.

Bi, Z., Gong, Q., Guo, P. and Cheng, Q. (2020), "Experimental study of the evolution of soil arching effect under cyclic loading based on trapdoor test and particle image velocimetry", *Can. Geotech. J.*, **57**, 903-920. https://doi.org/10.1139/cgj-2019-0205.

Biradar, J., Banerjee, S., Shankar, R., Ghosh, P., Mukherjee, S. and Fatahi, B. (2019), "Response of square anchor plates embedded in reinforced soft clay subjected to cyclic loading", *Geomech. Eng.*, **17**(2), 165-173. https://doi.org/10.12989/gae.2019.17.2.165.

Chevalier, B., Combe, G. and Villard, P. (2012), "Experimental and discrete element modeling studies of the trapdoor problem: influence of the macro-mechanical frictional parameters", *Acta Geotech.*, **7**(1), 15-39. https://doi.org/10.1007/s11440-011-0152-5.

Chevalier, B. and Otani, J. (2011), "Arching observation in three-dimensional trapdoor problem with X-ray CT and Discrete Element Method", *Soils Found.*, **51**(3), 459-469. https://doi.org/10.3208/sandf.51.459.

Eskişar, J., Otani, J. and Hironaka, J. (2012), "Visualization of soil arching on reinforced embankment with rigid piled foundation using X-ray CT", *Geotext. Geomembranes*, **32**, 44-54. https://doi.org/10.1016/j.geotexmem.2011.12.002.

Feng, S., Ai, S. and Chen, H. (2017), "Estimation of arching effect in geosynthetic-reinforced structures", *Comput. Geotech.*, **87**, 188-197. https://doi.org/10.1016/j.compgeo.2017.02.014.

Giroud, J.P., Bonaparte, R., Beech, J.F. and Gross, B.A. (1990), "Design of soil layer-geosynthetic systems overlying voids", *Geotext. Geomembranes*, **9**(1), 11-50. https://doi.org/10.1016/0266-1144(90)90004-V.

Han, G., Gong, Q. and Zhou, S. (2015), "Soil arching in a piled embankment under dynamic load", *Int. J. Geomech.*, **15**(6), 04014094. https://doi.org/10.1061/(ASCE)GM.1943-5622.0000443.

Han, J., Bhandari, A. and Wang, F. (2012), "DEM analysis of stresses and deformations of geogrid-reinforced embankments over piles", *Int. J. Geomech.*, **12**(4), 340-350. https://doi.org/10.1061/(ASCE)GM.1943-5622.0000050.

Han, J., Wang, F., Al-Naddaf, M. and Xu, C. (2017). "Progressive development of two-dimensional soil arching with displacement", *Int. J. Geomech.*, **17**(12), 04017112. https://doi.org/10.1061/(ASCE)GM.1943-5622.0001025.

Heitz, C., Lüking, J. and Kempfert, H.G. (2008), "Geosynthetic reinforced and pile supported embankments under static and cyclic loading", *Proceedings of EuroGeo4-fourth European Geosynthetics Conference*, Edinburgh, UK.

Huckert, A., Briançon, L., Villard, P. and Garcin, P. (2016), "Load transfer mechanisms in geotextile-reinforced embankments overlying voids: experimental and analytical approaches", *Geotext. Geomembranes*, **44**(3), 442-456. https://doi.org/10.1016/j.geotexmem.2015.06.005.

Iglesia, G.R., Einstein, H.H. and Whitman, R.V. (2014), "Investigation of soil arching with centrifuge tests", *J. Geotech.*

Geoenviron. Eng., **140**(2), 04013005. https://doi.org/10.1061/(ASCE)GT.1943-5606.0000998.

Iglesia, G.R. (1991), "Trapdoor experiments on the centrifuge: A study of arching in geomaterials and similitude in geotechnical models", Ph.D. Dissertation, Massachusetts Institute of Technology, MA, USA.

Jenck, O., Dias, D. and Kastner, R. (2005), "Soft ground improvement by vertical rigid piles two-dimensional physical modeling and comparison with current design methods", *Soils Found.*, **45**(6), 15-30. https://doi.org/10.3208/sandf.45.15.

Jenck, O., Dias, D. and Kastner, R. (2007), "Two-dimensional physical and numerical modeling of a pile-supported earth platform over soft soil", *J. Geotech. Geoenviron. Eng.*, **133**(3), 295-305. https://10.1061/(ASCE)1090-0241(2007)133:3(295).

Jesmani, M., Kamalzare, M. and Sarbandi, B.B. (2016), "Seismic response of geosynthetic reinforced retaining walls", *Geomech. Eng.*, **10**(5), 635-655. https://doi.org/10.12989/gae.2016.10.5.635.

Kahyaoglu, M.R. and Sahin, M. (2021), "Model studies on polymer strip reinforced soil retaining walls", *Geomech. Eng.*, **25**(5), 357-371. https://doi.org/10.12989/gae.2021.25.5.357.

Ladanyi, B. and Hoyaux, B. (1969), "A study of the trap-door problem in a granular mass", *Can. Geotech. J.*, **6**(1), 1-14. https://doi.org/10.1139/t69-001.

Lai, H., Zheng, J., Cui, M. and Chu, J. (2020), "'Soil arching" for piled embankments: Insights from stress redistribution behaviour of DEM modelling", *Acta Geotech.*, **15**(8), 2117-2136. https://doi.org/10.1007/s11440-019-00902-x.

Lai, H., Zheng, J., Zhang, J., Zhang, R. and Cui, L. (2014), "DEM analysis of "soil"-arching within geogrid-reinforced and unreinforced pile-supported embankments", *Comput. Geotech.*, **61**, 13-23. https://doi.org/10.1016/j.compgeo.2014.04.007.

Liang, L., Xu, C., Chen, Q. and Chen, Q. (2020), "Experimental and theoretical investigations on evolution of soil-arching effect in 2D trapdoor problem", *Int. J. Geomech.,* **20**(6), 06020007. https://doi.org/10.1061/(ASCE)GM.1943-5622.0001643.

Liu, H.B., Yang, G.Q., Wang, H. and Xiong B.L. (2017), "A large-scale test of reinforced soil railway embankment with soilbag facing under dynamic loading", *Geomech. Eng.*, **12**(4), 579-593. https://doi.org/10.12989/gae.2017.12.4.579.

McNulty, J.W. (1965), "An experimental study of arching in sand", Ph.D. Dissertation, Department of civil engineering, University of Illinois, USA.

Mittal, S. and Meyase, K. (2012), "Study for improvement of grounds subjected to cyclic loads", *Geomech. Eng.*, **4**(3), 191-208. https://doi.org/10.12989/gae.2012.4.3.191.

Moradi, G. and Abbasnejad, A. (2015), "Experimental and numerical investigation of arching effect in sand using modified Mohr Coulomb", *Geomech. Eng.*, **8**(6), 829-844. https://doi.org/10.12989/gae.2015.8.6.829.

Nguyen, T. and Tran, L.V. (2021), "Arching effect in sand piles under base deflection using geometrically non-linear isogeometric analysis", *Geomech. Eng.*, **26**(4), 369-384. https://doi.org/10.12989/gae.2021.26.4.369.

Rebello, N.E., Shivashankar, R. and Sastry, V.R. (2018), "Surface displacements due to tunneling in granular soils in presence and absence of geosynthetic layer under footings", *Geomech. Eng.*, **15**(2), 739-744. https://doi.org/10.12989/gae.2018.15.2.739.

Rui, R., Han, J., van Eekelen, S.J.M. and Wan, Y. (2019), "Experimental investigation of soil-arching development in unreinforced and geosynthetic-reinforced pile-supported embankments", *J. Geotech. Geoenviron. Eng.*, **145**(1), 04018103. https://doi.org/10.1061/(ASCE)GT.1943-5606.0002000.

Rui, R., Han, J., Ye, Y., Chen, C. and Zhai, Y. (2020), "Load transfer mechanisms of granular cushion between column foundation and rigid raft", *Int. J. Geomech.*, **20**(1), 04019139. https://doi.org/10.1061/(ASCE)GM.1943-5622.0001539.

Rui, R., van Tol, A., Xia, X., van Eekelen, S., Hu, G. and Xia, Y. (2016b), "Evolution of soil arching: 2D DEM simulations", *Comput. Geotech.*, **73**, 199-209. https://doi.org/10.1016/j.compgeo.2015.12.006.

Rui, R., van Tol, A.F., Xia, Y.Y., van Eekelen, S.J.M. and Hu, G. (2016a), "Investigation of soil-arching development in dense sand by 2D model tests", *Geotech. Test. J.*, **39**(3), 1-16. https://10.1520/GTJ20150130.

Shen, P., Xu, C. and Han, J. (2020), "Centrifuge tests to investigate global performance of geosynthetic-reinforced pile-supported embankments with side slopes", *Geotext. Geomembranes*, **48**(1), 120-127. https://doi.org/10.1016/j.geotexmem.2019.103527.

Terzaghi, K. (1936), "Stress distribution in dry and in saturated sand above a yielding trap-door", *Proceedings of the 1st International Conference on Soil Mechanics and Foundation Engineering*, Cambridge.

Terzaghi, K. (1943), Theoretical Soil Mechanics, John Wiley and Sons, Inc. New York, NY, USA.

van Eekelen, S.J.M,. Bezuijen, A., Lodder, H.J. and van Tol, A.F. (2012), "Model experiments on piled embankments. Part I", *Geotext. Geomembranes*, **32**, 69-81. https://doi.org/10.1016/j.geotexmem.2011.11.002.

Wang, F., Han, J., Miao, L.C. and Bhandari, A. (2009), "Numerical analysis of geosynthetic-bridged and drilled shaft-supported embankments over large sinkhole", *Geosynth. Int.*, **16**(6), 408-419. https://doi.org/10.1680/gein.2009.16.6.408.

Wang, H.L. and Chen, R.P. (2019), "Estimating static and dynamic stresses in geosynthetic-reinforced pile-supported track-bed undertrain moving loads", *J. Geotech. Geoenviron. Eng.*, **145**(7), 04019029. https://doi.org/10.1061/(ASCE)GT.1943-5606.0002056.

White, D.J., Take, W.A. and Bolton, M.D. (2003), "Soil deformation measurement using particle image velocimetry (PIV) and photogrammetry", *Géotechnique*, **53**(7), 619-631. https://doi.org/10.1680/geot.2003.53.7.619.

Won, M.S., Lee, O.H. and Kim, Y.S. (2016), "A 12-year long-term study on the external deformation behavior of Geosynthetic Reinforced Soil (GRS) walls", *Geomech. Eng.*, **10**(5), 565-575. https://doi.org/ 10.12989/gae.2016.10.5.565.

Xu, C., Luo, M., Shen, P., Han, J. and Ren, F. (2020), "Seismic performance of a whole Geosynthetic Reinforced Soil – Integrated Bridge System (GRS-IBS) in shaking table test", *Geotext. Geomembranes*, **48**(3), 315-330. https://doi.org/10.1016/j.geotexmem.2019.12.004.

Xu, C., Song, S. and Han, J. (2016), "Scaled model tests on influence factors of full geosynthetic-reinforced pile-supported embankments", *Geosynth. Int.*, **23**(2), 140-153. https://doi.org/10.1680/jgein.15.00038.

Xu, C., Zhang, X., Han, J. and Yang, Y. (2019), "Two-dimensional soil-arching behavior under static and cyclic loading", *Int. J. Geomech.*, **19**(8), 04019091. https://doi.org/10.1061/(ASCE)GM.1943-5622.0001482.

Zhang, Z., Tao, F., Han, J., Ye, G., Cheng, B. and Liu, L. (2021a), "Influence of surface footing loading on soil arching above multiple buried structures in transparent sand", *Can. J. Civ. Eng.*, **48**, 124-133. https://doi.org/10.1139/cjce-2019-0352.

Zhang, Z., Tao, F.J., Han, J., Ye, G.B. and Cheng, B.N. (2021b), "Arching development in transparent soil during multiple trapdoor movement and surface footing loading", *Int. J. Geomech.*, **21**(3), 04020262. https://doi.org/10.1061/(ASCE)GM.1943-5622.0001908.

Zhao, Y., Gong, Q., Wu, Y., Zornberg, J.G., Tian, Z. and Zhang, X. (2021), "Evolution of active arching in granular materials: Insights from load, displacement, strain, and particle flow", *Powder Technol.*, **384**, 160-175.

https://doi.org/10.1016/j.powtec.2021.02.011.

IC